IEEE Access
Multidisciplinary | Rapid Review | Open Access Journal

Received 5 April 2024, accepted 23 April 2024, date of publication 6 May 2024, date of current version 14 May 2024.

Digital Object Identifier 10.1109/ACCESS.2024.3397186

RESEARCH ARTICLE

Optically-Transparent EM Skins for Outdoor-to-Indoor mm-Wave Wireless Communications

GIACOMO OLIVERI[1], (Fellow, IEEE), FRANCESCO ZARDI[1], GIORGIO GOTTARDI[1], AND ANDREA MASSA[1,2,3,4], (Fellow, IEEE)

[1]ELEDIA Research Center (ELEDIA@UniTN), Department of Civil, Environmental, and Mechanical Engineering (DICAM), University of Trento, 38123 Trento, Italy
[2]ELEDIA Research Center (ELEDIA@UESTC), School of Electronic Science and Engineering, University of Electronic Science and Technology of China, Chengdu 611731, China
[3]ELEDIA Research Center (ELEDIA@TSINGHUA), Tsinghua University, Haidian, Beijing 100084, China
[4]School of Electrical Engineering, Tel Aviv University, Tel Aviv 69978, Israel

Corresponding author: Andrea Massa (andrea.massa@unitn.it)

This work supported in part by the National Science Foundation of China under the Chang-Jiang Visiting Professorship Program through the Project SPEED under Grant 61721001; in part by the European Union-NextGenerationEU within the PNRR Program through the Project "National Centre for HPC, Big Data and Quantum Computing (CN HPC)" under Grant CUP: E63C22000970007; in part by the Italian Ministry of Education, Universities and Research (MUR) (Departments of Excellence 2023–2027) through the Project DICAM-EXC under Grant L232/2016; and in part by the Italian Ministry for Universities and Research within the PRIN-PNRR 2022 Program through the Project "AURORA-Smart Materials for Ubiquitous Energy Harvesting, Storage, and Delivery in Next Generation Sustainable Environments."

ABSTRACT Optically-transparent opportunistic electromagnetic skins (*OTO-EMS*s) are proposed to enable outdoor-to-indoor (*O2I*) millimeter-wave (*mmW*) wireless communications with existing windows/glass-panels. More in detail, static passive *EMS*s consisting of optically-transparent conducting patterned layers attached to standard glass-panels are designed. Towards this end, both the phase coverage and the optical transparency of a meshed copper-based meta-atom printed on a non-dedicated insulated glass substrate are optimized. Successively, the feasibility of *OTO-EMS*s able to support *mmW* high-efficiency *O2I* transmissions along non-Snell refraction directions is numerically demonstrated also through full-wave simulations.

INDEX TERMS Static passive EM skins, smart electromagnetic environment, next-generation communications, metamaterials, metasurfaces, mmWave communications, transparent conductors, meshed copper.

I. INTRODUCTION AND RATIONALE

The deployment of wireless cellular systems operating at millimeter wave (*mmW*) frequencies has been proposed as a suitable technological solution for the ever-increasing demand for high data rates in mobile communications [1], [2], [3]. As a matter of fact, the availability of a wide spectrum in the *mmW* band potentially supports several Gbps of peak data rates, while still employing relatively simple user terminals [1]. However, major propagation challenges need to be addressed if outdoor-to-indoor (*O2I*) operations are of interest [1], [4]. Indeed, the signal degradation caused by the building penetration losses can prevent the establishment of a *O2I* link in most practical scenarios [1], [4], [5]. For instance, penetration loss values exceeding 40 dB have been measured through outdoor glass-panels at 28 [GHz] [1], [5]. Similar results have been obtained when dealing with concrete or brick walls, as well [1]. To compensate for these losses, additional indoor base stations or higher transmitting powers may be used [1], [5], but such strategies would imply a non-trivial increase in the network complexity, the operational costs, and the energy consumption.

An intriguing alternative is the inclusion in the building walls of passive field manipulating devices to "route" the

The associate editor coordinating the review of this manuscript and approving it for publication was Davide Ramaccia.

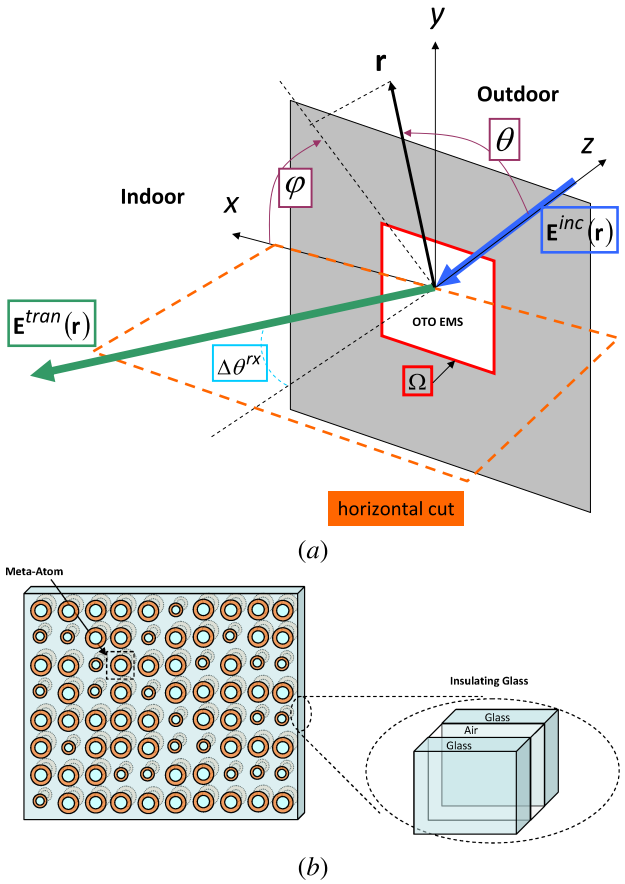

FIGURE 1. Sketch of (*a*) the *O2I* scenario at hand and (*b*) the *OTO-EMS* architecture.

electromagnetic (*EM*) propagation according to the desired *O2I* paths [Fig. 1(*a*)]. Such an idea stems from the recent methodological and technological advances in surface *EM* and artificial 2D material engineering [6] at the basis of the Smart *EM* Environment (*SEME*) paradigm [7], [8], [9], [10], [11], [12], [13]. More specifically, a planar *EMS* capable of tailoring the refracted field may be designed so that the penetration loss through its surface is minimized and, additionally, the transmitted field propagates along a non-Snell direction [6]. A "traditional" design of such a transmitting *EMS* would typically require several conducting layers separated by a combination of air, foam, and/or dedicated substrates [6]. Moreover, and besides the non-negligible costs, substituting a portion of a wall or a window with such an *EMS* would be impractical because of both the visual impact and the structural/thermal insulation limitations.

To make sustainable *O2I* wireless communications at *mmW* frequencies, an opportunistic implementation is proposed in this paper. More specifically, the concept of optically-transparent opportunistic *EMS* (*OTO-EMS*) is introduced. An *OTO-EMS* is a static passive *EMS* that consists of one or more conducting, but optically-transparent, patterned layers which are attached using an optical clear adhesive (*OCA*)[1] to an *existing* glass window, this latter acting as an equivalent *EMS* support/substrate [Fig. 1(*b*)]. Accordingly, an *OTO-EMS* can be seamlessly installed on any existing window to establish a reliable *O2I* link at *mmW* frequencies by avoiding any visual/structural impact or thermal/acoustic insulation issues of traditional implementations.

Hereafter, the design of *OTO-EMS*s will be carried out by addressing the following implementation challenges:

- the design of a meta-atom[2] that, unlike state-of-the-art layouts for transmitting skins [6], combines a set of patterned transparent conductive layers and a non-dedicated glass-based substrate to yield a suitable phase coverage and a *mmW* transparency;
- the synthesis of finite *mmW* *OTO-EMS*s featuring anomalous wave manipulation capabilities (e.g., non-Snell refraction) and high aperture efficiencies.

To achieve these goals, a customized implementation of the System-by-Design (*SbD*) paradigm [15], recently demonstrated for standard reflecting *EMS* engineering [16], [17], [18], is used. More specifically, the meta-atom design process is based on a parametric approach featuring (*i*) an elementary geometrical layout and (*ii*) the exploitation of a standard commercial *insulating glass* (*IG*) as the *EMS* substrate, which consists of two glass panes separated by an air-filled region [Fig. 1(*b*)]. Furthermore, the optically-transparent conductors to realize the *EMS* patterning are realized with the *copper mesh* concept [19], [20], [21], [22], [23], [24] because of its better suitability for *mmW* applications and the relatively inexpensive implementation if compared to transparent conducting oxides [24] or liquid crystals [25]. The multi-atom structure composing the *EMS* is then optimized to fit macro-scale performance goals expressed in terms of transmitted field and optical transparency.

According to such a description and to the best of the authors' knowledge, the main novelties of this work with respect to the state of the art include (*i*) the use at *mmW* frequencies of static passive transmitting *EMS*s suitable as a retro-fitting option for existing windows/glass-panels; (*ii*) the opportunistic implementation of *EMS*s by exploiting the standard insulating glass as *EMS* substrate and featuring transparent conductors for the metallic patterning; (*iii*) the assessment of the effectiveness of the proposed *O2I* solution in terms of wave manipulation properties and achievable improvements with respect to standard glass-panels both in standard and non-Snell directions; (*iv*) the customization of the system-by-design synthesis method [15] to the case of transmitting *EMS*s, while state-of-the-art implementations refer to reflecting surfaces [16], [17], [18].

The outline of the paper is as follows. The design problem at hand is formulated in Sect. II, where the

[1] *OCA*s are typically based on acrylate chemistry, and exhibit electrical properties similar to glass [14]. Several *OCA* technologies and fabrication processes are commercially available [14].

[2] In the following, "meta-atom" and "unit cell" will be used as synonyms to identify the elementary *EMS* element, likewise in the recent literature on *SEME* [6], [8], [16], [17], [18].

OTO-EMS concept is introduced, as well. Section III reports a set of representative numerical results to show the features and to assess, also through full-wave simulations, the potentialities of *OTO-EMS*s as retro-fitting options of existing windows/glass-panels to support *O2I mmW* wireless communications. Finally, some conclusions are drawn (Sect. IV).

II. MATHEMATICAL FORMULATION

Let us consider the *O2I* wireless communications scenario in Fig. 1(*a*) where an outdoor source illuminates an *OTO-EMS*, which occupies a region Ω of a glass window, with an incident time-harmonic electromagnetic field $\mathbf{E}^{inc}$. This latter is locally modeled as a plane wave with wave vector $\mathbf{k}^{inc}$ and incidence direction $\left(\theta^{inc}, \varphi^{inc}\right)$. The field $\mathbf{E}^{tran}$ transmitted through the region Ω in a point $\mathbf{r}$ of *local* coordinates (x, y, z) depends on the vector $\mathcal{D}$ [i.e., $\mathbf{E}^{tran} = \mathbf{E}^{tran}(\mathbf{r}; \mathcal{D})$] of the geometrical/physical descriptors of the *EMS*

$$\mathcal{D} \triangleq \left\{ \underline{d}_{pq};\ p = 1, \ldots, P;\ q = 1, \ldots, Q \right\} \tag{1}$$

whose L-sized (p, q)-th $(p = 1, \ldots, P;\ q = 1, \ldots, Q)$ entry, $\underline{d}_{pq} \triangleq \left\{ d_{pq}^{(l)};\ l = 1, \ldots, L \right\}$, contains the features of the corresponding meta-atom including the *copper mesh* descriptors.

Under the assumption that the *O2I* transmission from other building portions (e.g., walls) is negligible, the synthesis of an *OTO-EMS* for establishing a reliable *O2I* wireless link can be formulated as the identification of the *EMS* descriptors $\mathcal{D}$ such that $\Phi\left[\mathbf{E}^{tran}(\mathbf{r}; \mathcal{D})\right]$ is minimized

$$\mathcal{D}^{opt} \triangleq \arg\left\{ \min_{\mathcal{D}} \left[\Phi\left[\mathbf{E}^{tran}(\mathbf{r}; \mathcal{D})\right] \right] \right\} \tag{2}$$

where $\Phi\left[\mathbf{E}^{tran}(\mathbf{r}; \mathcal{D})\right]$ is a cost function that encodes the macro-scale radiation objectives defined on the total transmitted pattern.

Regardless of the definition of Φ, a reliable methodology to evaluate $\mathbf{E}^{tran}(\mathbf{r}; \mathcal{D})$ is necessary. Towards this end, the full-wave modeling of the *OTO-EMS* could be adopted, but such an approach is practically infeasible due to the associated computational costs and even more if it had to be iteratively repeated for every guess of $\mathcal{D}$ as generally required in *SbD*-based design processes [15].

Consequently, an alternative semi-analytic state-of-the-art approach that leverages on the Love's equivalence principle and the homogenization of the surface currents [6], [16], [17], [18], [26], [27], [28], [29], [30] is adopted in the following. More specifically, the field transmitted through the region Ω in the far field is computed as follows [28] and [29]

$$\begin{aligned}\mathbf{E}^{tran}(\mathbf{r}; \mathcal{D}) &\approx \frac{jk_0}{4\pi} \frac{\exp(-jk_0|\mathbf{r}|)}{|\mathbf{r}|} \\ &\times \sum_{p=1}^{P} \sum_{q=1}^{Q} \widehat{\mathbf{r}}' \times \left[\eta_0 \widehat{\mathbf{r}}' \times \mathbf{J}_{pq}^{e}\left(\underline{d}_{pq}\right) + \mathbf{J}_{pq}^{m}\left(\underline{d}_{pq}\right) \right] \\ &\times \int_{\Omega_{pq}} \exp\left(jk_0 \widehat{\mathbf{r}} \cdot \mathbf{r}'\right) d\mathbf{r}'\end{aligned} \tag{3}$$

where $\widehat{\mathbf{r}}' \triangleq \frac{\mathbf{r}'}{|\mathbf{r}'|}$, k_0 and η_0 are the free-space wave-number and impedance, respectively,

$$\begin{cases} \mathbf{J}_{pq}^{e}\left(\underline{d}_{pq}\right) \approx \dfrac{1}{\eta_0} \widehat{\mathbf{z}} \times \mathbf{k}^{inc}\left(\mathbf{r}_{pq}\right) \times \left[\overline{\overline{T}}_{pq}\left(\underline{d}_{pq}\right) \cdot \mathbf{E}^{inc}\left(\mathbf{r}_{pq}\right) \right] \\ \mathbf{J}_{pq}^{m}\left(\underline{d}_{pq}\right) \approx \left[\overline{\overline{T}}_{pq}\left(\underline{d}_{pq}\right) \cdot \mathbf{E}^{inc}\left(\mathbf{r}_{pq}\right) \right] \times \widehat{\mathbf{z}} \end{cases} \tag{4}$$

are the electric/magnetic surface current coefficients in the pq-th meta-atom, $\mathbf{r}_{pq}$ is the barycenter of the pq-th meta-atom area,

$$\overline{\overline{T}}_{pq}\left(\underline{d}_{pq}\right) = \begin{bmatrix} T_{pq}\left(\underline{d}_{pq}\right)\Big|_{TE} & T_{pq}\left(\underline{d}_{pq}\right)\Big|_{TE/TM} \\ T_{pq}\left(\underline{d}_{pq}\right)\Big|_{TM/TE} & T_{pq}\left(\underline{d}_{pq}\right)\Big|_{TM} \end{bmatrix} \tag{5}$$

is the local complex transmission tensor [31] (also labeled as local dyadic transmission coefficient [29]) in the pq-th meta-atom, under the local periodicity approximation [16], with support Ω_{pq} $\left(\sum_{p=1}^{P}\sum_{q=1}^{Q} \Omega_{pq} \triangleq \Omega\right)$ of area Δ^2, Δ being the meta-atom lattice periodicity so that the *EMS* has a total area of $\mathcal{L}_x \times \mathcal{L}_y = (P \times \Delta) \times (Q \times \Delta)$.

According to (3), the macro-scale behaviour of an *OTO-EMS* depends on the magnitude and the phase of the $\overline{\overline{T}}_{pq}\left(\underline{d}_{pq}\right)$ entries, which are controlled by the user-defined micro-scale descriptors $\mathcal{D}$. However, unlike the synthesis of reflective *EMS*s [16], [17], [18], [28], additional difficulties arise for the *EMS* designer owing to the phase/magnitude limits of such entries [32]. As a matter of fact, while a single-layer patterning is sufficient to yield a full 360° phase coverage in reflecting *EMS*s [6], a transmitting *EMS* must theoretically include at least three layers of conducting material to do the same with a minimum of 50% of the transmission efficiency [32], unless Huygens' designs are considered [33], [34], [35], [36], [37]. On the other hand, the requirement of easy integration in existing windows of our *OTO-EMS* forces the meta-atom architecture to a two-layer metallic structure [Fig. 1(*b*)] with an intrinsic limitation in terms of transmission coefficient control.

According to the above formulation, it turns out that (*i*) $\mathbf{E}^{tran}$ is determined by the surface-current coefficients $\{\mathbf{J}_{pq}^{w}$ $(w = \{e, m\});\ p = 1, \ldots, P;\ q = 1, \ldots, Q\}$ according to the linear equation (3), while (*ii*) these latter, which satisfy (4), depend on the entries of $\overline{\overline{T}}_{pq}$ that are non-linearly related to the meta-atom descriptors $\underline{d}_{pq}$ [i.e., $\overline{\overline{T}}_{pq} = \overline{\overline{T}}\left(\underline{d}_{pq}\right)$]. Consequently and analogously to the guidelines adopted in the design of reflecting *EMS*s [16], [17], the *OTO-EMS* synthesis problem is split into two sub-problems: (1) the *OTO* meta-atom design and (2) the *OTO-EMS* layout synthesis.

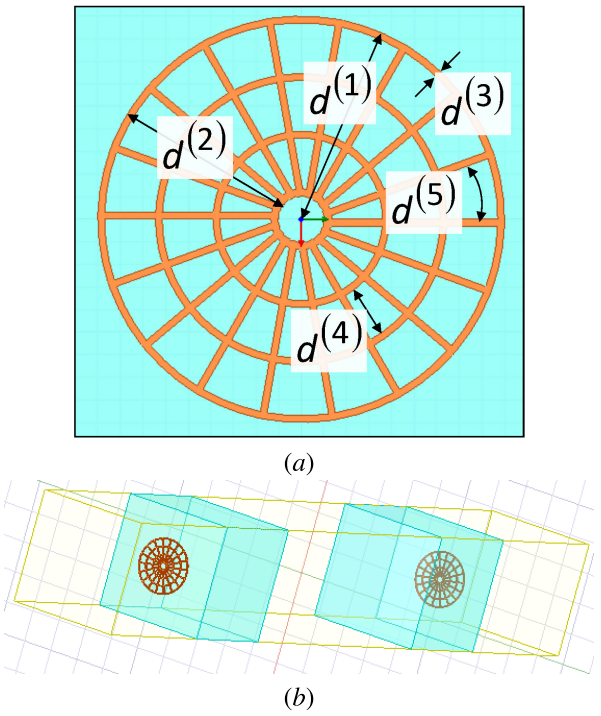

FIGURE 2. *OTO Meta-Atom Design* - **Picture of (*a*) the parametric representation of the unit cell and (*b*) the corresponding HFSS 3D model.**

A. OTO *META-ATOM DESIGN*

As for the former sub-problem (1), it is stated as follows

> ***OTO Meta-Atom Design Problem*** - Design a meta-atom structure and Ψ^{opt} so that $\Phi_{atom}(\Psi) = \left\{\sum_{i=TE,TM}\left[\alpha_i^{PC}\Phi_i^{PC}(\Psi) + \alpha_i^{MAG}\Phi_i^{MAG}(\Psi)\right] + \alpha^{OT}\Phi^{OT}(\Psi)\right\}^{-1}$ is minimized

where Ψ is the meta-atom feasibility set ($\Psi \triangleq \left\{\underline{d} : d_{\min}^{(l)} \le d^{(l)} \le d_{\max}^{(l)};\ l = 1,\ldots,L\right\}$), Φ_i^{PC} is the phase coverage of the unit cell on the i-th ($i = \{TE, TM\}$) field component [6] ($\Phi_i^{PC}(\Psi) \triangleq \max_{\underline{d}\in\Psi}\angle T_i\left(\underline{d}\right) - \min_{\underline{d}\in\Psi}\angle T_i\left(\underline{d}\right)$), Φ_i^{MAG} is the worst-case transmittance magnitude coefficient on the i-th field component ($\Phi_i^{MAG}(\Psi) = \min_{\underline{d}\in\Psi}\left[\left|T_i\left(\underline{d}\right)\right|\right]$), α_i^{PC} and α_i^{MAG} being the corresponding weights, while Φ^{OT} and α^{OT} are the optical transparency and the associated weight, respectively. It is worth remarking that both *TE* and *TM* modes have been included in the definition of $\Phi_{atom}(\Psi)$ since their effect has been considered in the subsequent results. Moreover, the definition of Φ^{OT} depends on both the meta-atom geometry (i.e., patterning layout) and the geometry of the conducting mesh. In this paper, it is computed as $\Phi^{OT}(\Psi) \triangleq \min_{\underline{d}\in\Psi}\left[\mathcal{T}_{atom}^{OTO}\left(\underline{d}\right)\right]$ where $\mathcal{T}_{atom}^{OTO}\left(\underline{d}\right)$ is the overall meta-atom optical transmittance [24].

The first step in solving the *OTO Meta-Atom Design Problem* is the choice of the meta-atom model and the corresponding unit cell descriptors $\underline{d}$. Towards this end, one should notice that, unlike other *EMS* design problems [6], the addressed scenario is strongly constrained since the amount of conducting material of the *copper mesh* patterning in the unit cell area has to be minimized for maximizing the optical transparency $\mathcal{T}$, while still allowing a suitable *mmW* field transmission control. Moreover, the layout of the unit cell has to enable a direct installation on commercial *IG* windows with non-customized thicknesses and profiles without the need for additional substrates/supports and/or any further mechanical operation such as vias drilling. On the other hand, as in antenna synthesis [38], [39], different codings of the structure at hand, including parametric and non-parametric descriptions [38], [39], imply different solution approaches.

According to such considerations, a canonical meta-atom geometry is chosen and a parametric coding of such a reference structure is adopted [6], [16]. The main motivation is that of demonstrating the feasibility of the *OTO-EMS* concept without the need for advanced meta-atom shaping and/or complex coding. More in detail, the dual-layer circular ring meta-atom [6] in Fig. 2 ($L = 5$) is adopted. In this case, the conductive copper mesh is implemented according to a conformal geometry combining circular and radial wires and it is printed on both sides of the glass [Fig. 2(*a*)]. The meta-atom descriptors are the outer ring radius $d^{(1)}$, the overall ring width $d^{(2)}$, the mesh wire radius $d^{(3)}$, the mesh radial gap $d^{(4)}$, and the mesh angular gap $d^{(5)}$ [Fig. 2(*a*)]. All the remaining features (i.e., the glass/air layer thickness and material properties) are user-defined constants. Moreover, each patterned layer is assumed to be attached to the outer surface of the glass panel [Fig. 2(*b*)] to make it suitable as a retro-fitting option for existing windows.

Thanks to these choices, the atom is expected to have good performance stability whatever the incident polarization [6], while yielding a low atom fill factor $\mathcal{F}_{atom}^{OTO}$ (i.e., the ratio between the conductive area and the meta-atom support), hence resulting in high optical transparency [24]. Numerically, it turns out that

$$\mathcal{F}_{atom}^{OTO} \approx \frac{\pi d^{(2)}\left[2d^{(1)} - d^{(2)}\right]}{\Delta^2}\mathcal{F}_{mesh}, \tag{6}$$

$\mathcal{F}_{mesh} \triangleq \frac{d^{(3)}}{d^{(3)}+d^{(4)}}$ being the mesh fill factor [24] that corresponds to an atom optical transmittance of $\mathcal{T}_{atom}^{OTO} = \left(1 - \mathcal{F}_{atom}^{OTO}\right)^4$ under the assumption of perfect transparency of the glass [24]. For comparison purposes, let us notice that $\mathcal{F}_{atom}^{OTO}$ is much lower than the fill-factor of standard *EMS* meta-atoms such as printed square patches [16], $\mathcal{F}_{atom}^{Patch} = \frac{\left[d^{patch}\right]^2}{\Delta^2}$, d^{patch} being the patch side.

As far as the design procedure is concerned, thanks to the reduced number of descriptors of the meta-atom [$L = 5$ - Fig. 2(*a*)], the responses of several guess meta-atoms belonging to different feasibility sets are full-wave simulated with Ansys HFSS [40] [Fig. 2(*b*)] until $\Phi_{atom}(\Psi) \le \eta_{atom}$, η_{atom} being a user-chosen threshold.

B. OTO-EMS *LAYOUT SYNTHESIS*

Concerning the sub-problem (2), it can be formulated as follows

OTO-EMS Layout Synthesis Problem - Given $\mathbf{E}^{inc}(\mathbf{r})$, find $\mathbf{J}^{w}_{opt}(\mathbf{r};\mathcal{D})$ $(w = \{e,m\})$ and the corresponding $\mathcal{D}^{opt}$ such that $\Phi\left[\mathbf{E}^{tran}(\mathbf{r};\mathcal{D})\right]$ is minimized

where $\mathbf{E}^{tran}$ is semi-analytically computed as in (3) starting from (4) and using the values of the local transmission tensor $\overline{\overline{T}}$ in correspondence with the *OTO* meta-atom feasibility set Ψ^{opt} deduced in sub-problem (1) [i.e., $\overline{\overline{T}} = \overline{\overline{T}}\left(\underline{d}_{pq}\right)$, $\underline{d}_{pq} \in \Psi^{opt}$].

It is worthwhile to point out that the proposed *OTO-EMS* synthesis approach, which separates the meta-atom design [*Sub-Problem* (1)] from the *EMS* layout synthesis [Sub-Problem (2)], allows one to deal with a wide variety of different problems, each being formulated by re-defining the cost function Φ, without the need to re-engineer the unit cell structure.

The synthesis of an *OTO-EMS* layout fitting a macro-scale radiation objective requires the explicit definition of the associated cost function Φ. Analogously to [18], this paper considers the power-maximization towards a receiver located in a position $\mathbf{r}^{rx}$. Therefore, the cost function Φ is given by

$$\Phi\left[\mathbf{E}^{tran}(\mathbf{r};\mathcal{D})\right] \triangleq \frac{1}{\left|\mathbf{E}^{tran}(\mathbf{r}^{rx};\mathcal{D})\right|}. \tag{7}$$

In fact, from the physical perspective, the minimization of $\Phi\left[\mathbf{E}^{tran}(\mathbf{r};\mathcal{D})\right]$ implies to the maximization of $\left|\mathbf{E}^{tran}(\mathbf{r};\mathcal{D})\right|$ in the $\mathbf{r} = \mathbf{r}^{rx}$ location, which corresponds to the realization of a collimated transmitted beam towards the receiver. Consequently and likewise state-of-the-art approaches dealing with reflecting *EMS*s [16], [17], [18], the definition of the micro-scale descriptors $\mathcal{D}^{opt}$ is determined by means of a two-step process where (*a*) the ideal surface currents $\widetilde{\mathbf{J}}^{w}(\mathbf{r})$ $(w = \{e,m\})$ that minimize (7) are firstly deduced, then (*b*) $\mathcal{D}^{opt}$ is computed by solving the following current-matching problem

$$\mathcal{D}^{opt} = \arg\left\{\min_{\mathcal{D}}\left[\Upsilon(\mathcal{D})\right]\right\} \tag{8}$$

where $\Upsilon(\mathcal{D}) \triangleq \left\|\mathbf{J}^{w}(\mathbf{r};\mathcal{D}) - \widetilde{\mathbf{J}}^{w}(\mathbf{r})\right\|^2$.

In particular, Step (*a*) is addressed with the phase-conjugation method [18], [41], [42], [43] to yield

$$\arg\left\{\widetilde{J}_a\right\}^{w}_{pq} = -\arg\left[\int_{\Omega_{pq}} \exp\left(jk_0\widehat{\mathbf{r}}^{rx}\cdot\mathbf{r}'\right)d\mathbf{r}'\right] \tag{9}$$

$(w = \{e,m\}, a = \{x,y\}, p = 1,\ldots,P, q = 1,\ldots,Q)$ where $\widehat{\mathbf{r}}^{rx} = \{\sin\theta^{rx}\cos\varphi^{rx}, \sin\theta^{rx}\sin\varphi^{rx}, \cos\theta^{rx}\}$, $(\theta^{rx},\varphi^{rx})$ being the receiver direction. Such a method guarantees that all current terms are added in-phase at the focusing point so that (7) is intrinsically minimized.

Step (*b*) is dealt with a customized version of the *SbD* strategy [15], [16], [17], [18] that generates a succession of G iterations to identify $\mathcal{D}^{opt}$ (Fig. 3) [15]. At each g-th $(g = 1,\ldots,G)$ iteration, a set of I guess *EMS* configurations, $\left\{\mathcal{D}^{(i)}_g \triangleq \left\{\underline{d}_{pq}\right\}^{(i)}_g \in \Psi^{opt};\ p = 1,\ldots,P,\ q = 1,\ldots,Q\right\}$;

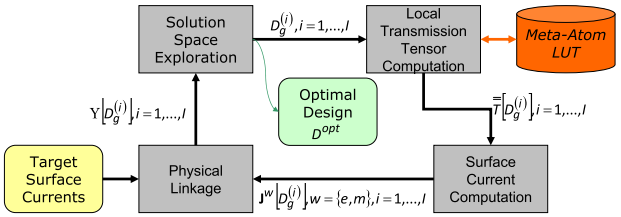

FIGURE 3. Flowchart of the customized SbD approach for the computation of $\mathcal{D}^{opt}$.

$i = 1,\ldots,I\}$ are generated by combining (*a*) a *solution-space-exploration* block, which is implemented in an in-house coded software according to the particle swarm paradigm [44]; (*b*) a *local transmission tensor look-up table* (*LUT*) block, which stores the non-linear meta-atom response $\overline{\overline{T}}\left(\underline{d}\right)$, $\underline{d} \in \Psi^{opt}$, computed through the full-wave simulation of its numerical model in Ansys HFSS [Fig. 2(*b*)]; (*c*) a *surface electric/magnetic current computation* block, which implements (4), and (*d*) a *physical linkage* block, which is responsible for the computation of $\Upsilon(\mathcal{D})$. Accordingly, the procedure is not directly interfaced with *Ansys HFSS*, but rather exploits the outcomes of its simulations as stored in the *LUT*. The entire process is repeated until a maximum number of steps (i.e., $g = G$) or a stationarity condition on the minimization of the cost function is reached [15], [16], [17], [18], [44]. The optimal *OTO-EMS* descriptors are then set as follows

$$\mathcal{D}^{opt} = \arg\left\{\min_{g=1,\ldots,G;i=1,\ldots,I}\left[\min\Upsilon\left(\mathcal{D}^{(i)}_g\right)\right]\right\}. \tag{10}$$

III. NUMERICAL RESULTS

The objective of this section is twofold. On the one hand, it is aimed at proving the feasibility of an *OTO* meta-atom that enables advanced *mmW*-frequency wave manipulation properties, while keeping good optical transparency (Sect. III-A). On the other hand, it is devoted to show the features of *OTO-EMS*s and to assess their performance in comparison with non-patterned glasses as well as empty windows (Sect. III-B).

Unless otherwise specified, the *OTO-EMS*s designs have been carried out at $f_0 = 26$ [GHz] by considering a $\left(\theta^{inc},\varphi^{inc}\right) = (0,0)$ [deg] incident φ-polarized wave that illuminates the *EMS* with a 1 [V/m] field magnitude. The standard $4-10-4$ *IG* has been assumed as benchmark substrate. It consists of two glass panes of thickness $\tau_{glass} = 4$ [mm], relative permittivity $\varepsilon_r = 5.5$ and loss tangent $\tan\delta = 3.0\times10^{-2}$, which are separated by an air-filled space $\tau_{air} = 10$ [mm] thick (with unitary relative permittivity), so that the total thickness is $\tau_{IG} = 18$ [mm] (i.e., $\tau_{IG} \approx 1.56\lambda$). The metalizations have been assumed to consist of copper with conductivity $\sigma = 5.8\times10^7$ [S/m] and thickness 30×10^{-6} [m]. The meta-atom lattice periodicity has been set to $\Delta = 3.7$ [mm] (i.e., $\Delta \approx 0.32\lambda$).

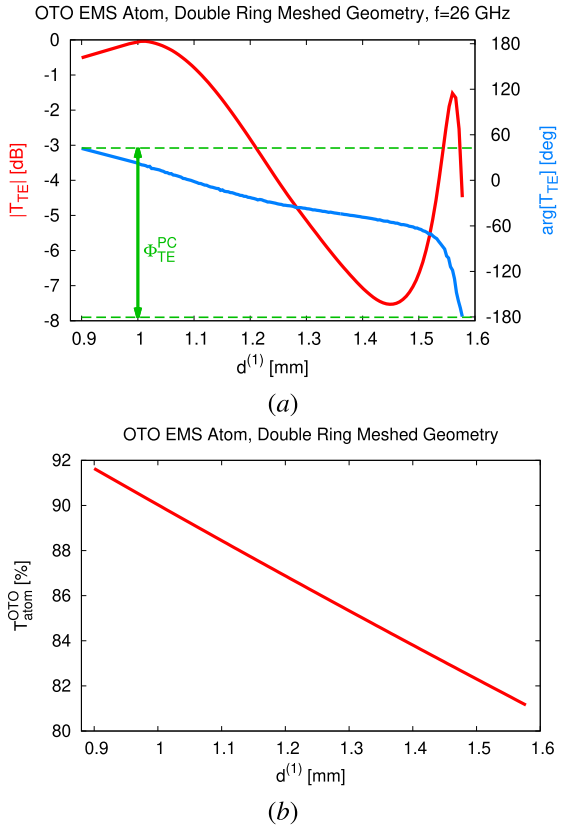

FIGURE 4. *OTO Meta-Atom Design* ($f_0 = 26$ [GHz]) - Plot of (*a*) the magnitude and the phase of T_{TE} $(\underline{d})$ and (*b*) the behaviour of the meta-atom transparency $\mathcal{T}_{atom}^{OTO}$ versus $d^{(1)}$.

A. OTO *META-ATOM DESIGN*

Following the guidelines detailed in Sect. II-A, the first task has been the design of an *OTO* meta-atom enabling advanced transmitted-field control properties subject to the constraint of being based on a minimum-complexity structure featuring transparent conducting layers patterned on a non-dedicated glass-based substrate.

Referring to the reference parametric model of the *EMS* unit cell in Fig. 2(*a*), the setup of the meshed copper (i.e., the patterning conductor) has been chosen according to [20] for yielding a mesh fill factor of about $\mathcal{F}_{mesh} \approx 11.7\%$, which corresponds to a single-layer conductor optical transmittance equal to $\mathcal{T}_{mesh} = (1 - \mathcal{F}_{mesh})^2 \approx 77.8\%$. More in detail, $d^{(3)} = 30 \times 10^{-6}$ [m] (i.e., the thickness of the mesh wires is roughly half of a typical human hair), $d^{(4)} = 225 \times 10^{-6}$ [m], and $d^{(5)} = 20$ [deg]. The meta-atom model has been then parametrically tuned to operate at f_0 by properly optimizing $d^{(1)}$ and $d^{(2)}$ [Fig. 2(*a*)]. By setting the trade-off ring width value $d^{(2)} = 795 \times 10^{-6}$ [m], $d^{(1)}$ has been chosen as the control parameter for the entries of $\overline{\overline{T}}$ [i.e., $\overline{\overline{T}}\left(\underline{d}\right) = \overline{\overline{T}}\left(d^{(1)}\right)$].

Figure 4(*a*) summarizes the transmission performance of the optimized meta-atom structure. It is worthwhile to point out that they have been predicted without considering equivalent homogenized models for the wire mesh

TABLE 1. *OTO Meta-Atom Design* ($f_0 = 26$ [GHz]) - Characteristics of the *OTO* meta-atom and comparison with the state-of-the-art.

Design	f_0 [GHz]	N	*IG?*	$\mathcal{T}_{atom}^{OTO}$ [%]	Φ_{TE}^{PC} [deg]	Φ_{TE}^{MAG} [dB]
Ideal $N = 2$	n.a.	2	n.a.	n.a.	230	-3.0
[46]	38.5	2	No	90	123	-1.5
[47]	28	2	No	95	196	-3.0
[48]	28.5	3	No	n.a.	290	-3.0
This work	26	2	Yes	80	220	-7.7

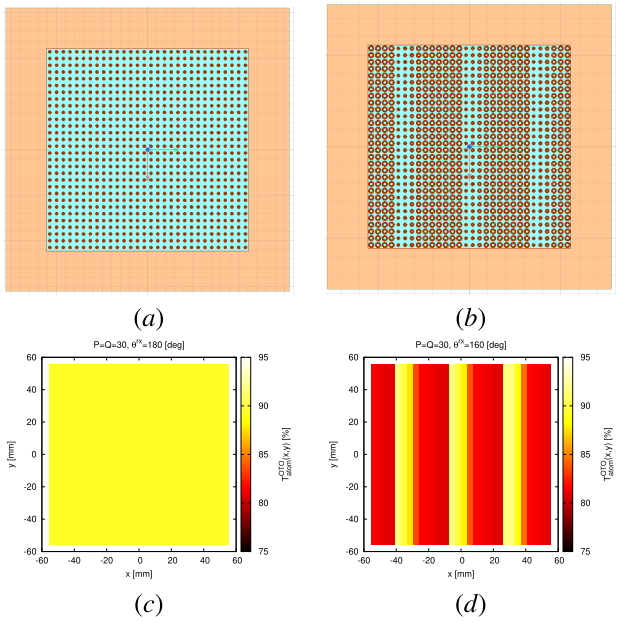

FIGURE 5. *OTO-EMS Layout Synthesis* ($f_0 = 26$ [GHz], $P = Q = 30$) - Plot of (*a*)(*b*) the *OTO-EMS* layouts and (c)(*d*) the corresponding optical transparency index when (*a*)(c) $\theta^{rx} = 180$ [deg] and (*b*)(*d*) $\theta^{rx} = 160$ [deg].

(i.e., the actual copper wire structure has been simulated in *Ansys HFSS*). It turns out that when varying $d^{(1)}$ within its feasibility range $d_{\min}^{(1)} \leq d^{(1)} \leq d_{\max}^{(1)}$ being $d_{\min}^{(1)} = 0.9 \times 10^{-3}$ [m] and $d_{\max}^{(1)} = 1.6 \times 10^{-3}$, such a unit cell supports a phase coverage of approximately $\Phi_{TE}^{PC} \approx 220$ [deg] with a worst-case transmittance magnitude of $\Phi_{TE}^{MAG} \approx -7.7$ [dB] [Fig. 4(*a*)].[3] The effects of the meta-atom insertion loss on the *OTO-EMS*s performance are assessed in the subsequent subsection. However, let us notice that the theoretical maximum phase range enabled by a non-transparent ideal two-layer meta-atom is around 230 [deg] for a 50% transmission efficiency [6], [32] (Tab. 1). Potential solutions to improve such performance while keeping the glass panel configuration may thus require increasing the number meta-atom layers as well as employing optimized inter-layer spacings [32].

[3]The same behavior holds true for the *TM* component owing to the cell symmetry, while the magnitude of the cross-polar components turns out < -30 [dB].

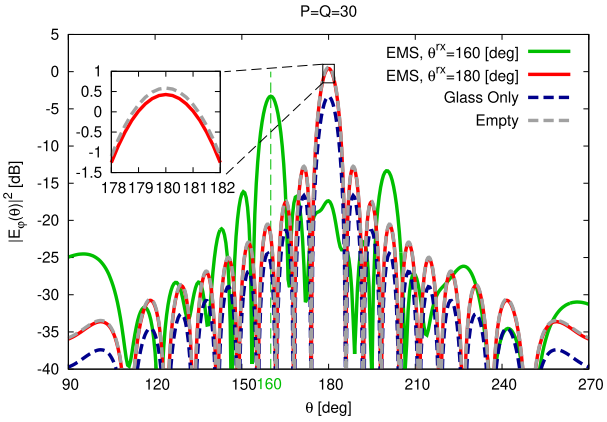

FIGURE 6. *OTO-EMS Layout Synthesis* - ($f_0 = 26$ [GHz], $P = Q = 30$, $\varphi^{rx} = 0$ [deg]) - Plots of the transmitted pattern, $\left|E_{\varphi}^{tran}(\mathbf{r})\right|^2$, versus θ.

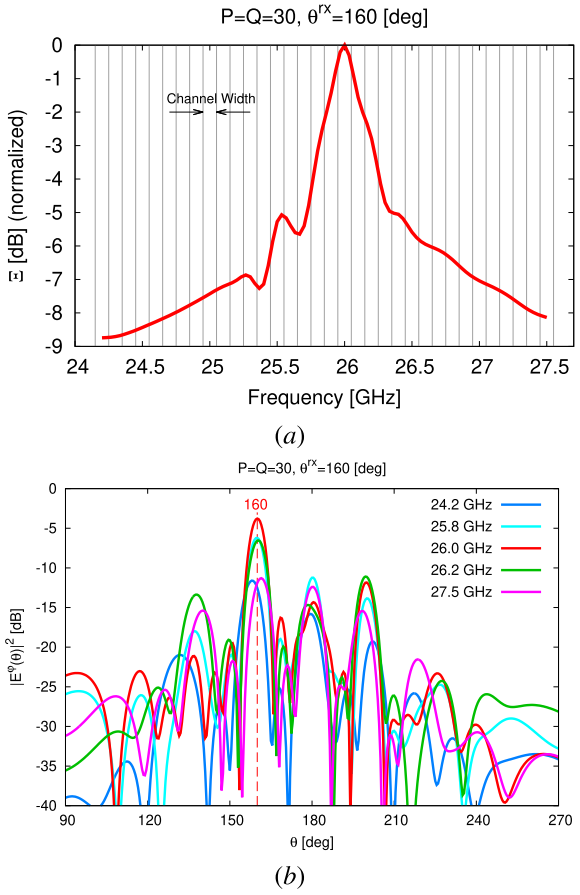

FIGURE 7. *OTO-EMS Layout Synthesis* - ($f_0 \in [24.2, 27.5]$ [GHz], $P = Q = 30$, $\theta^{rx} = 160$ [deg], $\varphi^{rx} = 0$ [deg]) - Plots of (*a*) the peak power pattern, Ξ, versus f_0 and (*b*) the transmitted pattern, $\left|E_{\varphi}^{tran}(\mathbf{r})\right|^2$, versus θ.

As regards the relation between $\overline{\overline{T}}$ and $d^{(1)}$ [Fig. 4(*a*)], it is worth noticing that the observed sensitivity is consistent with that of standard meta-atom architectures at such frequencies [45], [46], [48] and compliant with current generation *PCB* fabrication processes.

As for the transparency of the arising meshed meta-atom, the dependence of its optical transmittance on $d^{(1)}$ is shown in Fig. 4(*b*). The plot indicates that $\mathcal{T}_{atom}^{OTO} > 80\%$ regardless of the meta-atom setup within its feasibility range (i.e., $\underline{d} \in \Psi^{opt}$). This confirms the potentialities of meshed copper meta-atoms [19], [20], [21], [22], [23], [24] for building printed optically-transparent *EMS*s [Fig. 4(*b*)]. A comparison of the essential performance metrics and compliancy with *IG* installation (i.e., "*IG*?" column in Tab. 1) of the proposed *OTO* meta-atom with those of state-of-the-art transparent architectures featuring different number of metalization layers N is provided in Tab. 1, for the sake of completeness.

B. OTO-EMS LAYOUT SYNTHESIS

The first test case of this section, which is devoted to analyze the *O2I* transmission performance of *OTO-EMS*s, deals with the synthesis of a square *EMS* $\mathcal{L} \approx 11.1$ [cm]-sided ($P = Q = 30$) transmitting the wave towards $(\theta^{rx}, \varphi^{rx}) = (180, 0)$ [deg] (i.e., no anomalous transmission). The *OTO-EMS* layout, synthesized with the procedure of Sub-Sect. II-B, presents a uniform pattern with all cells identical [Fig. 5(*a*)] as expected from the Generalized Snell's Law for refraction [6]. The corresponding local optical transparency map [Fig. 5(*c*)] is uniform, as well, with a constant value of $\mathcal{T}_{atom}^{OTO}$ around 90% across the whole *EMS* support Ω.

Figure 6 compares the behaviour of the magnitude[4] of the dominant φ-component of the electric field $\left|E_{\varphi}^{tran}(\mathbf{r})\right|^2$ transmitted in the horizontal cut [$\varphi = 0$ [deg] - Fig. 1(*a*)] when applying the *OTO-EMS* in Fig. 5(*a*) [Fig. 6 (red line)] and when considering either non-patterned *IG* panel of the same size ["Glass only" - Fig. 6 (blue dashed line)] or when considering a hollow region of identical size Ω ["Empty" - Fig. 6 (grey dashed line)]. One can clearly infer that the *OTO-EMS* patterning considerably improves the transmitted power with respect to the standard commercial *IG* window of the same size (i.e., $\frac{\left|E_{\varphi}^{EMS}(\theta)\right|^2_{\theta=180\,deg}}{\left|E_{\varphi}^{Glass}(\theta)\right|^2_{\theta=180\,deg}} \approx 3.7$ [dB] - Fig. 6). Moreover, interested readers should notice that, despite the architectural and material constraints, such a meshed *EMS* features a power loss only 0.16 [dB] below the ideal hollow case (Fig. 6), while the beam-width size is equal since it depends on the panel aperture Ω.

The possibility to derive an *OTO-EMS* that supports anomalous transmission angles, with an adequate control of the transmitted beam, is validated next by keeping the same scenario of the previous example, but now considering an anomalous transmission angle of $\Delta\theta^{rx} = 20$ [deg] ($\Delta\theta^{rx} \triangleq 180 - \theta^{rx}$; $\theta^{rx} = 160$ [deg]). Figure 5(*b*) shows the synthesized *OTO-EMS* layout, while the plot of

[4]In the following, no normalization has been applied to the plotted quantities (i.e., the far-region electrical field magnitude has been reported) unless otherwise specified.

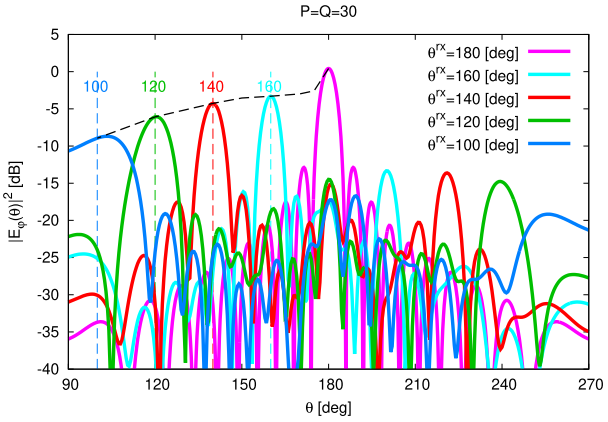

FIGURE 8. *OTO-EMS Layout Synthesis* - ($f_0 = 26$ [GHz], $P = Q = 30$, $\varphi^{rx} = 0$ [deg]) - Plots of the transmitted pattern, $\left|E_{\varphi}^{tran}(\mathbf{r})\right|^2$, versus θ.

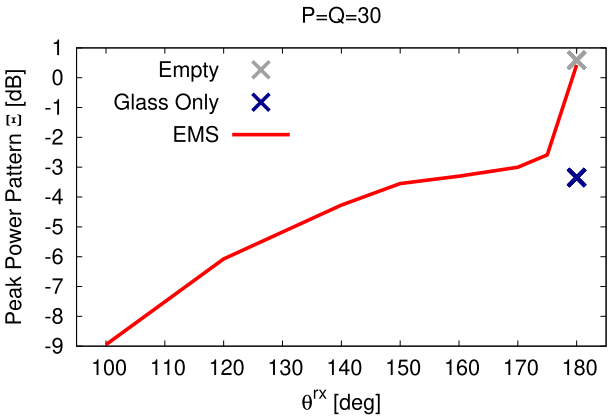

FIGURE 9. *OTO-EMS Layout Synthesis* - ($f_0 = 26$ [GHz], $P = Q = 30$, $\varphi^{rx} = 0$ [deg]) - Plots of the peak power pattern, Ξ, versus θ^{rx}.

$\mathcal{T}_{atom}^{OTO}(x, y)$ is reported in Fig. 5(*d*). This latter indicates that an excellent local transparency is achieved across the entire *EMS* support Ω since always $\mathcal{T}_{atom}^{OTO} > 80\%$. More importantly, the transmitted pattern along the horizontal cut in Fig. 6 (green line) proves that the *OTO-EMS* focuses the energy towards the anomalous direction by yielding an acceptable scan loss ($\frac{\left|E_{\varphi}^{EMS}(\theta)\right|^2_{\theta=160[deg]}}{\left|E_{\varphi}^{EMS}(\theta)\right|^2_{\theta=180[deg]}} \approx -3.6$ [dB] - Fig. 6), which is unavoidable because of the planar nature of the *EMS* as well as the insertion loss performance of the designed meta-atom [Fig. 4(*a*)].

The presence of moderate quantization side-lobes (e.g., $\theta \approx 200$ [deg] - Fig. 6), unlike the "non-anomalous transmission" case, is due to the limited phase coverage of the two-layer meta-atom at hand [Fig. 4(*a*)]. In fact, the designed *OTO-EMS*, featuring 14 different unit cell configurations,[5] yields an average 12.7 [deg] phase error with respect to the optimal phase profile. Of course, a better side-lobe control may be obtained whether exploiting multi-layer structures, but this would not be compliant with the retro-fitting constraint of the problem at hand.

The bandwidth performance of the proposed *OTO-EMS*s architecture is assessed in the subsequent numerical experiment. To this end, the previous $\Delta\theta^{rx} = 20$ [deg] design is analyzed considering the n258 5G *mmW* band (i.e., $f_0 \in [24.2, 27.5]$ [GHz]). The plot of the peak power pattern Ξ (i.e., $\Xi \triangleq \max_{\theta,\varphi}\left|E_{\varphi}^{tran}(\mathbf{r})\right|^2$) shows that, as expected owing to the resonant nature of the conceived meta-atom (Fig. 2), the skin efficiency reduces when the illumination frequency deviates from the nominal $f = 26$ [GHz], with a worst-case transmitted power reduction of ≈ 9 [dB] at the n258 band edges [Fig. 7(*a*)]. However, such losses are below 3 dB in 5 n258 band channels [i.e., 100 MHz-wide bands centered in the carrier frequencies $f_0 = \{25.8, 25.9, 26.0, 26.1, 26.2\}$ [GHz] - Fig. 7(*a*)]. It is worth remarking that such results have been obtained without re-optimizing the unit cell architecture (Fig. 2) on a broader band. Moreover, the designed structure still exhibits a collimated transmission (i.e., a well-defined main lobe) in the desired θ^{rx} direction in the entire n258 band [e.g., $f_0 = 24.2$ [GHz]; $f_0 = 27.5$ [GHz] - Fig. 7(*b*)].

The next test case analyzes the performance degradation versus the scan angle. Towards this end, a set of *OTO-EMS*s has been designed by varying the anomalous transmission angle in the range $\Delta\theta^{rx} \in \{40, 60, 80\}$ [deg] ($\theta^{rx} \in \{140, 120, 100\}$ [deg]). By comparing the transmitted beams in Fig. 8, the following outcomes can be drawn: (*i*) it is possible to yield an effective beam focusing despite the limited phase coverage of the *OTO* meta-atom and even when the scan angle is close to end-fire [e.g., $\Delta\theta = 80$ [deg], $\theta^{rx} = 100$ [deg] - Fig. 8 (blue line)]; (*ii*) regardless of the scan angle, the presence of moderate quantization lobes is confirmed, the major side-lobe usually appearing specularly to the orthogonal transmission angle (i.e., $\theta \approx 180 + \Delta\theta^{rx}$); (*iii*) as expected, there is the unavoidable beam broadening effect when the transmission angle gets closer to end-fire (e.g., blue vs. red line - Fig. 8) as well as an increase of the scan loss. This latter phenomenon is pointed out in Fig. 9 where the plot of the peak power pattern Ξ versus θ^{rx} is shown. As it can be observed, the scan loss sharply grows as θ^{rx} deviates from $\theta^{rx} = 180$ [deg]. This is actually caused by the presence of the quantization lobes in the beam pattern as well as the lower efficiency caused by insertion loss of the different unit cells [Fig. 4(*a*)], unlike the "non-anomalous transmission" case where all the meta-atoms are identical and therefore the design can be implemented exploiting the meta-atom with the best wireless efficiency [e.g., Fig. 8 (magenta line)].

The transmitted pattern of a window only partially covered by an *OTO-EMS* is numerically evaluated next. Towards this end, the previously designed $P = Q = 30$, $\Delta\theta^{rx} = 60$ [deg] ($\theta^{rx} = 120$ [deg]) skin is assumed to be installed at

[5]The number of different unit cells has not been constrained in the synthesis process, unlike the methods in [46] and [47], but likewise many state-of-the-art design strategies for static passive *EMS*s [6], [16], [17], [18], [28], [29], [45], [48], [49].

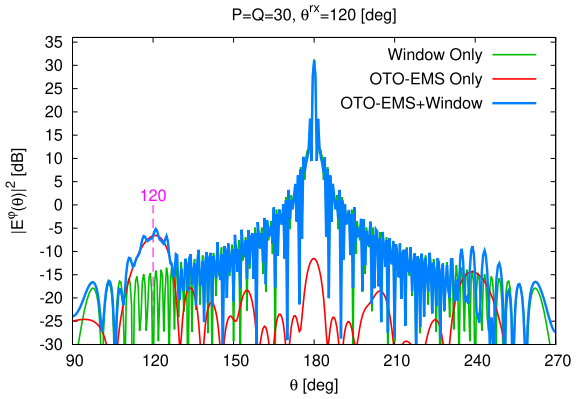

FIGURE 10. *OTO-EMS Layout Synthesis* - ($f_0 = 26$ [GHz], $P = Q = 30$, $\theta^{rx} = 120$ [deg], $\varphi^{rx} = 0$ [deg]) - Plots of the transmitted pattern, $\left|E_{\varphi}^{tran}(\mathbf{r})\right|^2$, versus θ when considering a glass window pane of aperture 0.6×1.1 [m^2].

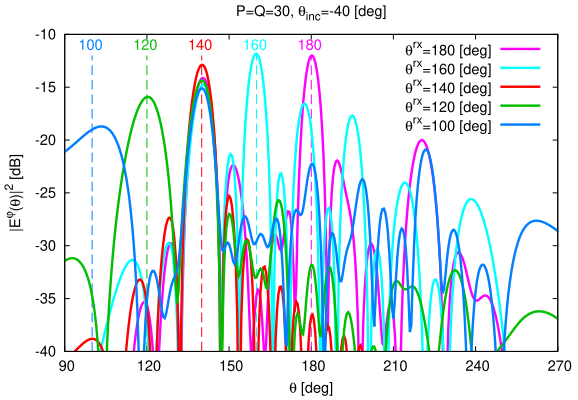

FIGURE 11. *OTO-EMS Layout Synthesis* - ($f_0 = 26$ [GHz], $P = Q = 30$, $\left(\theta^{inc}, \varphi^{inc}\right) = (-40, 0)$ [deg], $\varphi^{rx} = 0$ [deg]) - Plots of the transmitted pattern, $\left|E_{\varphi}^{tran}(\mathbf{r})\right|^2$, versus θ.

the center of a window pane of aperture 0.6×1.1 [m^2]. The plot of the transmitted patterns through the window alone (green line - Fig. 9), the *OTO-EMS* alone (red line - Fig. 10), or through their combination (red line - Fig. 10) shows that even a small skin panel (i.e., $\mathcal{L} \approx 11.1$ [cm]) enables to generate a collimated beam in the desired θ^{rx} direction which is > 37 dB above the power pattern generated by the window itself in $\theta = \theta^{rx}$ and approximately 8 dB above the sidelobe envelope (blue vs. green line - Fig. 10).

The behaviour of the conceived *OTO-EMS*s when dealing with oblique incidence angles is addressed in the subsequent numerical experiment. To this end, the design process has been carried out assuming $\theta^{inc} = -40$ [deg] and setting $\Delta\theta^{rx} \in \{0, 20, 40, 60, 80\}$ [deg] ($\theta^{rx} \in \{180, 160, 140, 120, 100\}$ [deg]). The results reported in Fig. 11 indicates that, despite the unavoidable quantization lobe in the $\theta = 140$ [deg] direction caused by the phase coverage limitations of the two-layer meta-atom at hand [Fig. 4(*a*)], the synthesized *OTO-EMS*s always support a collimated transmitted beam in the θ^{rx} direction even though $\theta^{inc} \neq 0$ [deg] (Fig. 11).

In the next example, the dependence of the transmission/focusing performance on the panel aperture is assessed. By setting $\Delta\theta^{rx} = 40$ [deg] (i.e., $\theta^{rx} = 140$ [deg]), the panel side has been varied in the range $7.4 \leq \mathcal{L} \leq 74$ [cm] (i.e., $20 \leq P \leq 200$ and $P = Q$). The plots of the peak power pattern Ξ versus the aperture size [Fig. 12(*a*)] indicate that the transmitted power focused by the *OTO-EMS* grows proportionally to the panel aperture as logically expected [e.g., $\frac{\Xi_{\mathcal{L}=74\,cm}}{\Xi_{\mathcal{L}=7.4\,cm}} \approx 39.9$ dB - Fig. 12(*a*)]. On the other hand, the comparison with the maximum power transmitted along broadside by either a non-patterned *IG* panel of the same size [“Glass only” - Fig. 12(*a*) (blue line)] or by a hollow region of identical aperture [“Empty” - Fig. 12(*a*) (grey line)] provides a key proof of the effectiveness of the *OTO-EMS* concept in *mmW O2I* communications. Indeed, it turns out that the synthesized patterned windows support transmission along anomalous angles (e.g., $\Delta\theta^{rx} = 40$ [deg]) with a power focusing efficiency which is less than 5 [dB] below the theoretical optimum (i.e., the power transmitted in the Snell’s direction through the hollow region), despite the unavoidable scan losses and the limited phase coverage of the meta-atom fulfilling retrofitting constraints.

For completeness, the plots of the transmitted beam patterns of representative apertures [i.e., $P \in \{20, 30, 80, 200\}$ and $P = Q$] are reported together with the broadside case (i.e., $\Delta\theta^{rx} = 0$ [deg]) in Fig. 12(*b*) to confirm previous considerations on (*a*) the presence and the location of the quantization lobes, (*b*) the beam-width dependence on the panel aperture, and (*c*) the improvement of the power transmission when widening Ω [Fig. 12(*b*)].

The subsequent numerical experiment deals with a more complex setup, the impinging wave being deflected in a double-anomalous direction (i.e., a non-Snell direction both in elevation and azimuth). More in detail, a $P = Q = 40$ meta-atoms *OTO-EMS* has been designed by imposing the *O2I* transmission along the direction ($\theta^{rx} = 140$ [deg], $\varphi^{rx} = 30$ [deg]). Also in this case, the synthesized *OTO-EMS* features a local optical transparency greater than 80% within the entire aperture Ω [Fig. 13(*a*)]. Moreover, the color map of the transmitted pattern in the $u - v$ coordinates shows that the *OTO-EMS* focuses the transmitted beam along the desired direction since $u^{rx} \approx 0.556$ and $v^{rx} \approx 0.321$ [Fig. 13(*b*)], being $u \triangleq \sin(\theta)\cos(\varphi)$ and $v \triangleq \sin(\theta)\sin(\varphi)$ the cosine directions [41]. Because of the limited phase coverage of the dual-layer meta-atom and analogously to single-anomalous transmissions, a specular quantization side-lobe appears at $u = -u^{rx}$, $v = -v^{rx}$. Such quantization lobes may be reduced by considering more complex meta-atom architectures enabling wider phase coverages.

The exploitation of the same theoretical framework when dealing with more complex illuminations is then analyzed. To this end, a 15 [dB]-gain horn antenna [Fig. 14(*a*)] located at 100 [m] from the *OTO-EMS* and

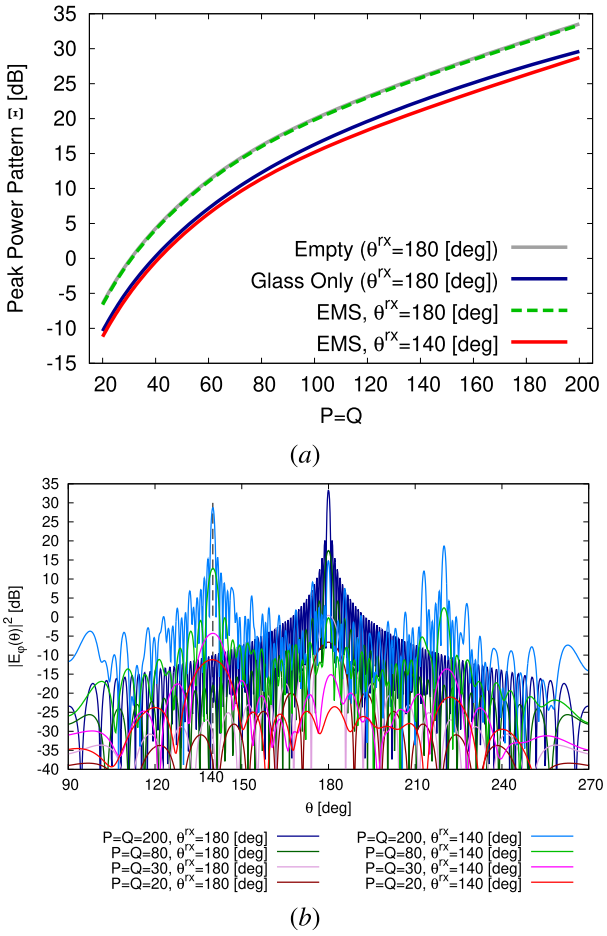

FIGURE 12. *OTO-EMS Layout Synthesis* - ($f_0 = 26$ [GHz], $\varphi^{rx} = 0$ [deg]) - Behaviour of (*a*) the peak power pattern, Ξ, versus P ($P = Q$) and plot of (*b*) the transmitted pattern, $\left|E_{\varphi}^{tran}(\mathbf{r})\right|^2$, versus θ when $\Delta\theta^{rx} \in \{0, 40\}$ [deg].

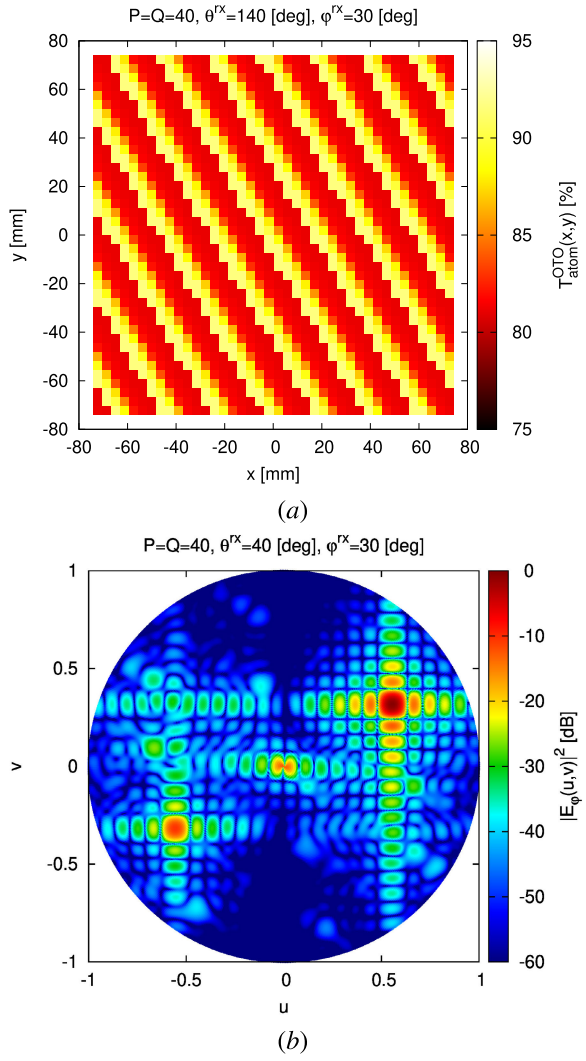

FIGURE 13. *OTO-EMS Layout Synthesis* - ($f_0 = 26$ [GHz], $P = Q = 30$, $\theta^{rx} \in 140$ [deg], $\varphi^{rx} = 30$ [deg]) - Plot of (*a*) the profile of the optical transparency index within Ω and (*b*) the transmitted pattern, $\left|E_{\varphi}^{tran}(\mathbf{r})\right|^2$, in the $u - v$ plane.

$\left(\theta^{inc}, \varphi^{inc}\right) = (-10, 0)$ [deg] has been used as a benchmark radiator to model a primary source (e.g., a base station), and the *OTO-EMS* design has been carried out enforcing $\Delta\theta^{rx} \in \{0, 20, 40, 60, 80\}$ [deg] ($\theta^{rx} \in \{180, 160, 140, 120, 100\}$ [deg]) [Fig. 14(*b*)]. The plots of the resulting patterns confirm that the beam shaping capabilities of the *OTO-EMS*s do not depend on the type of illumination [Fig. 14(*b*)]. In fact, the desired anomalous transmission is achieved regardless of the incident field [Fig. 14(*b*)].

The possibility to address more complex beamforming conditions exploiting *OTO-EMS*s has been investigated next. To this end, a sidelobe level (*SLL*)-constrained *OTO-EMS* synthesis process following the guidelines in [16] has been implemented on a $P \times Q = 30 \times 30$, $\left(\theta^{inc}, \varphi^{inc}\right) = (0, 0)$ [deg], $(\theta^{rx}, \varphi^{rx}) = (180, 0)$ [deg] design. More in detail, the design has been carried out enforcing a peak sidelobe $SLL \triangleq \frac{\max_{\theta \notin \Theta_{ML}} \left|E_{\varphi}^{tran}(\mathbf{r})\right|^2}{\max_{\theta \in \Theta_{ML}} \left|E_{\varphi}^{tran}(\mathbf{r})\right|^2}$ (Θ_{ML} being the mainlobe region) of $SLL = -20$ dB. The comparison of the normalized $\left|E_{\varphi}^{tran}(\mathbf{r})\right|^2$ for the "unconstrained" and "*SLL* constrained" designs show that a *SLL* mitigation can be achieved (i.e., $SLL_{constr} - SLL_{unconstr} = -5$ dB - Fig. 15) by slightly enlarging the mainlobe width, as theoretically expected (Fig. 15) and already demonstrated for reflecting *EMS*s [16].

The final test case is aimed at assessing the *OTO-EMS* performance in the presence of realistic non-ideal effects such as diffraction from edges, surface waves, and non-periodic mutual coupling that may arise in an *OTO-EMS* prototype. Towards this end, a full-wave analysis of an *OTO-EMS* has been carried out exploiting an industry-standard commercial simulator (*Ansys HFSS* [40]). A finite *OTO-EMS* model consisting of $P \times Q = 20 \times 20$ cells [Fig. 16(*a*)] and designed to operate with $\left(\theta^{inc}, \varphi^{inc}\right) = (-40, 0)$ [deg], $(\theta^{rx}, \varphi^{rx}) = (160, 0)$ [deg]) has been implemented considering a finite-element boundary-integral (*FE-BI*) formulation

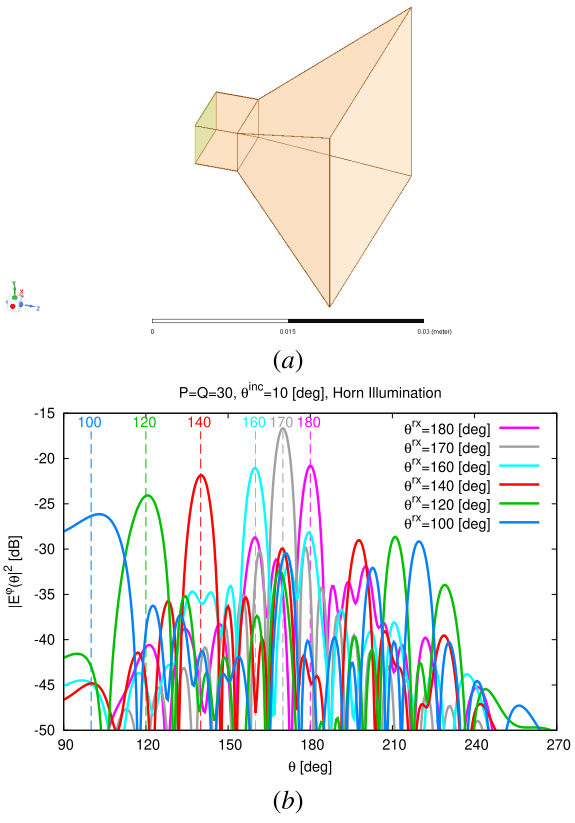

FIGURE 14. *OTO-EMS Layout Synthesis* - ($f_0 = 26$ [GHz], $P = Q = 30$, $\left(\theta^{inc}, \varphi^{inc}\right) = (-10, 0)$ [deg], $\varphi^{rx} = 0$ [deg], *Horn Illumination*) - Plots of the transmitted pattern, $\left|E_{\varphi}^{tran}(\mathbf{r})\right|^2$, versus θ.

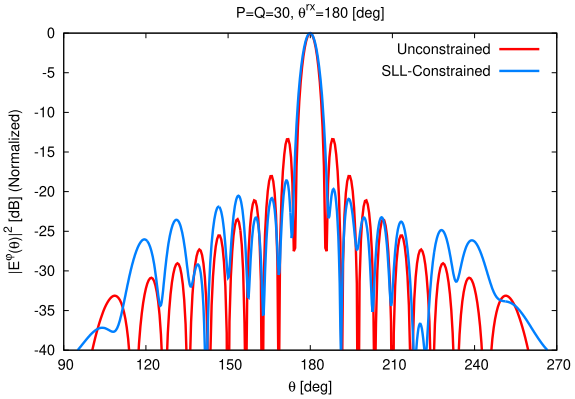

FIGURE 15. *OTO-EMS Layout Synthesis* - ($f_0 = 26$ [GHz], $P = Q = 30$, $(\theta^{rx}, \varphi^{rx}) = (180, 0)$ [deg]) - Comparison of the plots of the normalized transmitted pattern, $\left|E_{\varphi}^{tran}(\mathbf{r})\right|^2$, versus θ, for unconstrained vs. sidelobe-constrained design.

to avoid any numerical approximation resulting from periodic boundary conditions. The plot of the analytically-computed pattern positively compare with the full-wave simulated one [Fig. 16(*b*)]. More specifically, both the main beam location/magnitude and the sidelobe location and envelope is confirmed by the full-wave simulation [Fig. 16(*b*)],

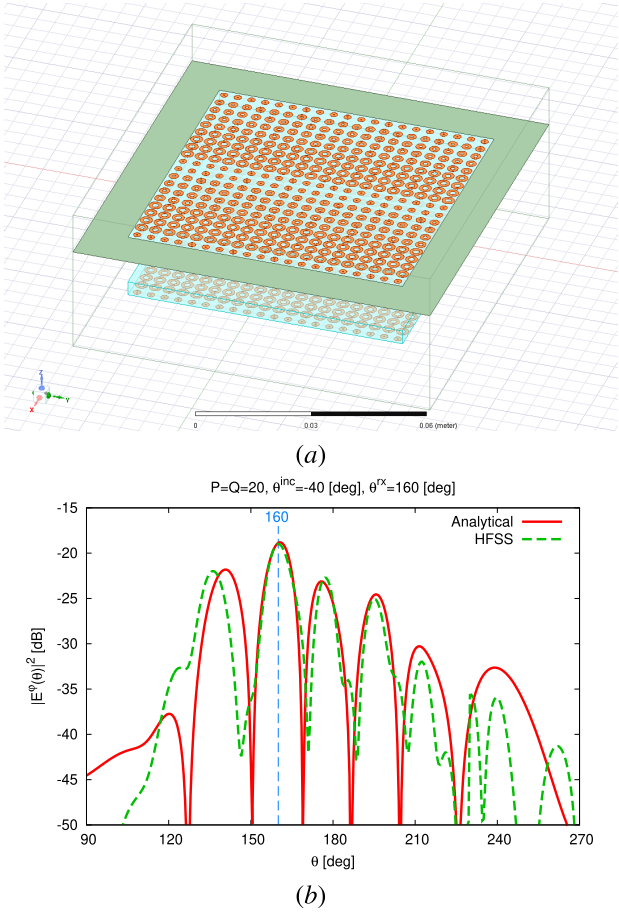

FIGURE 16. *OTO-EMS Full-Wave Validation* - ($f_0 = 26$ [GHz], $P = Q = 20$, $\left(\theta^{inc}, \varphi^{inc}\right) = (-40, 0)$ [deg], $(\theta^{rx}, \varphi^{rx}) = (160, 0)$ [deg]) - 3D Model (*a*) and plot of the analytical and Ansys HFSS-simulated transmitted pattern, $\left|E_{\varphi}^{tran}(\mathbf{r})\right|^2$, versus θ (*b*).

with a minor mismatch in the angular regions close to endfire possibly related to truncation effects and surface waves [Fig. 16(*b*)]. Such a result, which is consistent with the typical accuracy of state-of-the-art formulations [29], supports the previous considerations regarding the *OTO-EMS* concept.

IV. CONCLUSION

*OTO-EMS*s have been proposed as a profitable technological solution to enable *O2I* wireless communications at *mmW* frequencies. They consist of conducting optically-transparent patterned layers attached to *existing* glass windows to minimize both costs and visual impacts by also allowing an easy deployment. Full-wave numerical simulations of synthesized *OTO-EMS*s of finite sizes have assessed the feasibility as well as the effectiveness of *O2I* transmissions along both Snell and non-Snell refraction angles at *mmW*.

Accordingly, the fundamental methodological advancements of this work include (*i*) the demonstration of the feasibility of mmWave transparent *EMS*s suitable as a

retro-fitting option for existing windows / glass panels; (*ii*) the assessment of the *OTO-EMS*s features in terms of wave control also in comparison with non-patterned glass panels and addressing both standard and non-Snell focusing as well as sidelobe mitigation; (*iii*) the adaptation of the *SbD* synthesis concept to the case of transmitting *EMS* which generalizes existing implementations based on reflecting structures [16], [17], [18].

Future works, beyond the scope of the current paper and also currently impossible in our university owing to the lack of suitable resources and facilities for the realization and the measurement of the resulting devices at *mmW* frequencies, will be aimed at prototyping and measuring, in a controlled environment, the synthesized *OTO-EMS* samples. Towards this end, fabrication approaches previously employed in metalens design such as [46], [47], and [48] may be generalized/customized to the scenario at hand. Nevertheless, the presented full-wave simulation results obtained using an industry-standard commercial software (*Ansys HFSS* [40]) provide a preliminary evaluation of the impact of non-idealities such as diffraction from edges, surface waves, and non-periodic mutual coupling on the features of a practical *OTO-EMS*.

ACKNOWLEDGMENT

The author Andrea Massa wishes to thank E. Vico for her never-ending inspiration, support, guidance, and help.

REFERENCES

[1] T. S. Rappaport, Y. Xing, G. R. MacCartney, A. F. Molisch, E. Mellios, and J. Zhang, "Overview of millimeter wave communications for fifth-generation (5G) wireless networks—With a focus on propagation models," *IEEE Trans. Antennas Propag.*, vol. 65, no. 12, pp. 6213–6230, Dec. 2017.

[2] W. Hong, K.-H. Baek, and S. Ko, "Millimeter-wave 5G antennas for smartphones: Overview and experimental demonstration," *IEEE Trans. Antennas Propag.*, vol. 65, no. 12, pp. 6250–6261, Dec. 2017.

[3] T. S. Rappaport, G. R. MacCartney, S. Sun, H. Yan, and S. Deng, "Small-scale, local area, and transitional millimeter wave propagation for 5G communications," *IEEE Trans. Antennas Propag.*, vol. 65, no. 12, pp. 6474–6490, Dec. 2017.

[4] I. Rodriguez, H. C. Nguyen, T. B. Sorensen, J. Elling, J. A. Holm, P. Mogensen, and B. Vejlgaard, "Analysis of 38 GHz mmWave propagation characteristics of urban scenarios," in *Proc. Eur. Wireless 21st Eur. Wireless Conf.*, May 2015, pp. 1–8.

[5] T. S. Rappaport, S. Sun, R. Mayzus, H. Zhao, Y. Azar, K. Wang, G. N. Wong, J. K. Schulz, M. Samimi, and F. Gutierrez, "Millimeter wave mobile communications for 5G cellular: It will work!" *IEEE Access*, vol. 1, pp. 335–349, 2013.

[6] F. Yang and Y. Rahmat-Samii, *Surface Electromagnetics With Applications in Antenna, Microwave, and Optical Engineering*, Cambridge, U.K.: Cambridge Univ. Press, 2019.

[7] A. Massa, A. Benoni, P. Da Rù, S. K. Goudos, B. Li, G. Oliveri, A. Polo, P. Rocca, and M. Salucci, "Designing smart electromagnetic environments for next-generation wireless communications," *Telecom*, vol. 2, no. 2, pp. 213–221, May 2021.

[8] F. Yang, D. Erricolo, and A. Massa, "Guest editorial smart electromagnetic environment," *IEEE Trans. Antennas Propag.*, vol. 70, no. 10, pp. 8687–8690, Oct. 2022.

[9] M. Barbuto, Z. Hamzavi-Zarghani, M. Longhi, A. Monti, D. Ramaccia, S. Vellucci, A. Toscano, and F. Bilotti, "Metasurfaces 3.0: A new paradigm for enabling smart electromagnetic environments," *IEEE Trans. Antennas Propag.*, vol. 70, no. 10, pp. 8883–8897, Oct. 2022.

[10] M. D. Renzo, M. Debbah, D.-T. Phan-Huy, A. Zappone, M.-S. Alouini, C. Yuen, V. Sciancalepore, G. C. Alexandropoulos, J. Hoydis, H. Gacanin, J. D. Rosny, A. Bounceur, G. Lerosey, and M. Fink, "Smart radio environments empowered by reconfigurable AI meta-surfaces: An idea whose time has come," *EURASIP J. Wireless Commun. Netw.*, vol. 2019, no. 1, pp. 1–20, Dec. 2019.

[11] M. Di Renzo, A. Zappone, M. Debbah, M.-S. Alouini, C. Yuen, J. de Rosny, and S. Tretyakov, "Smart radio environments empowered by reconfigurable intelligent surfaces: How it works, state of research, and the road ahead," *IEEE J. Sel. Areas Commun.*, vol. 38, no. 11, pp. 2450–2525, Nov. 2020.

[12] M. Di Renzo, K. Ntontin, J. Song, F. H. Danufane, X. Qian, F. Lazarakis, J. De Rosny, D.-T. Phan-Huy, O. Simeone, R. Zhang, M. Debbah, G. Lerosey, M. Fink, S. Tretyakov, and S. Shamai (Shitz), "Reconfigurable intelligent surfaces vs. relaying: Differences, similarities, and performance comparison," *IEEE Open J. Commun. Soc.*, vol. 1, pp. 798–807, 2020.

[13] C. Huang, A. Zappone, G. C. Alexandropoulos, M. Debbah, and C. Yuen, "Reconfigurable intelligent surfaces for energy efficiency in wireless communication," *IEEE Trans. Wireless Commun.*, vol. 18, no. 8, pp. 4157–4170, Aug. 2019.

[14] J. T. Abrahamson, H. Z. Beagi, F. Salmon, and C. J. Campbell, *Optically Clear Adhesives for Foldable OLED Displays: Requirements, Failure Modes and Solutions*. Saint Paul, MN, USA: 3M Company, 2000. [Online]. Available: https://multimedia.3m.com/mws/media/1793258O/optically-clear-adhesives-for-foldable-oled-displays-whitepaper.pdf

[15] A. Massa and M. Salucci, "On the design of complex EM devices and systems through the system-by-design paradigm: A framework for dealing with the computational complexity," *IEEE Trans. Antennas Propag.*, vol. 70, no. 2, pp. 1328–1343, Feb. 2022.

[16] G. Oliveri, P. Rocca, M. Salucci, and A. Massa, "Holographic smart EM skins for advanced beam power shaping in next generation wireless environments," *IEEE J. Multiscale Multiphys. Comput. Techn.*, vol. 6, pp. 171–182, 2021.

[17] G. Oliveri, F. Zardi, P. Rocca, M. Salucci, and A. Massa, "Building a smart EM environment–AI-enhanced aperiodic micro-scale design of passive EM skins," *IEEE Trans. Antennas Propag.*, vol. 70, no. 10, pp. 8757–8770, Oct. 2022.

[18] G. Oliveri, M. Salucci, and A. Massa, "Generalized analysis and unified design of EM skins," *IEEE Trans. Antennas Propag.*, vol. 71, no. 8, pp. 6579–6592, Aug. 2023.

[19] S. K. Sharma, D. Zhou, A. Luttgen, and C. D. Sarris, "A micro copper mesh-based optically transparent triple-band frequency selective surface," *IEEE Antennas Wireless Propag. Lett.*, vol. 18, pp. 202–206, 2019.

[20] S. H. Kang and C. W. Jung, "Transparent patch antenna using metal mesh," *IEEE Trans. Antennas Propag.*, vol. 66, no. 4, pp. 2095–2100, Apr. 2018.

[21] Y. He and G. V. Eleftheriades, "A thin double-mesh metamaterial radome for wide-angle and broadband applications at millimeter-wave frequencies," *IEEE Trans. Antennas Propag.*, vol. 68, no. 3, pp. 2176–2185, Mar. 2020.

[22] Z. J. Silva and C. R. Valenta, "Evaluating optically transparent conductors at RF and microwave frequencies: A new figure of merit," *IEEE Microw. Wireless Compon. Lett.*, vol. 31, no. 4, pp. 349–352, Apr. 2021.

[23] J. P. Lombardi, R. E. Malay, J. H. Schaffner, H. J. Song, M.-H. Huang, S. C. Pollard, M. D. Poliks, and T. Talty, "Copper transparent antennas on flexible glass by subtractive and semi-additive fabrication for automotive applications," in *Proc. IEEE 68th Electron. Compon. Technol. Conf. (ECTC)*, May 2018, pp. 2107–2115.

[24] Z. J. Silva, C. R. Valenta, and G. D. Durgin, "Optically transparent antennas: A survey of transparent microwave conductor performance and applications," *IEEE Antennas Propag. Mag.*, vol. 63, no. 1, pp. 27–39, Feb. 2021.

[25] H. Kim, J. Kim, and J. Oh, "Communication a novel systematic design of high-aperture-efficiency 2D beam-scanning liquid-crystal embedded reflectarray antenna for 6G FR3 and radar applications," *IEEE Trans. Antennas Propag.*, vol. 70, no. 11, pp. 11194–11198, Nov. 2022.

[26] C. A. Balanis, *Advanced Engineering Electromagnetics*. New York, NY, USA: Wiley, 1989.

[27] A. Epstein and G. V. Eleftheriades, "Huygens' metasurfaces via the equivalence principle: Design and applications," *J. Opt. Soc. Amer. B, Opt. Phys.*, vol. 33, no. 2, p. A31, 2016.

[28] G. Oliveri, F. Zardi, P. Rocca, M. Salucci, and A. Massa, "Constrained design of passive static EM skins," *IEEE Trans. Antennas Propag.*, vol. 71, no. 2, pp. 1528–1538, Feb. 2023.
[29] M. J. Mencagli, E. Martini, S. Maci, and M. Albani, "A physical optics approach to the analysis of metascreens," *IEEE Access*, vol. 8, pp. 162634–162641, 2020.
[30] S. Pearson and S. V. Hum, "Optimization of electromagnetic metasurface parameters satisfying far-field criteria," *IEEE Trans. Antennas Propag.*, vol. 70, no. 5, pp. 3477–3488, May 2022.
[31] F. S. Cuesta, I. A. Faniayeu, V. S. Asadchy, and S. A. Tretyakov, "Planar broadband Huygens' metasurfaces for wave manipulations," *IEEE Trans. Antennas Propag.*, vol. 66, no. 12, pp. 7117–7127, Dec. 2018.
[32] A. H. Abdelrahman, A. Z. Elsherbeni, and F. Yang, "Transmission phase limit of multilayer frequency-selective surfaces for transmitarray designs," *IEEE Trans. Antennas Propag.*, vol. 62, no. 2, pp. 690–697, Feb. 2014.
[33] J.-W. Lian, Y.-L. Ban, and Y. J. Guo, "Wideband dual-layer Huygens' metasurface for high-gain multibeam array antennas," *IEEE Trans. Antennas Propag.*, vol. 69, no. 11, pp. 7521–7531, Nov. 2021.
[34] S. L. Jia, X. Wan, D. Bao, Y. J. Zhao, and T. J. Cui, "Independent controls of orthogonally polarized transmitted waves using a Huygens metasurface," *Laser Photon. Rev.*, vol. 9, no. 5, pp. 545–553, Sep. 2015.
[35] L. W. Wu, H. F. Ma, Y. Gou, R. Y. Wu, Z. X. Wang, M. Wang, X. Gao, and T. J. Cui, "High-transmission ultrathin Huygens' metasurface with 360° phase control by using double-layer transmitarray elements," *Phys. Rev. Appl.*, vol. 12, no. 2, Aug. 2019, Art. no. 024012.
[36] C. Xue, Q. Lou, and Z. N. Chen, "Broadband double-layered Huygens' metasurface lens antenna for 5G millimeter-wave systems," *IEEE Trans. Antennas Propag.*, vol. 68, no. 3, pp. 1468–1476, Mar. 2020.
[37] D. Su, H. Zhang, H. Xiao, W. Song, H. Xiong, D. Xiao, and X. Wang, "A double-layer metal-only Huygens' metasurface transmitarray," *IEEE Antennas Wireless Propag. Lett.*, vol. 22, no. 8, pp. 1897–1901, Aug. 2023.
[38] C.-C. Lin, Y.-C. Kan, L.-C. Kuo, and H.-R. Chuang, "A planar triangular monopole antenna for UWB communication," *IEEE Microw. Wireless Compon. Lett.*, vol. 15, no. 10, pp. 624–626, Oct. 2005.
[39] J. M. Johnson and Y. Rahmat-Samii, "Genetic algorithms and method of moments (GA/MOM) for the design of integrated antennas," *IEEE Trans. Antennas Propag.*, vol. 47, no. 10, pp. 1606–1614, Oct. 1999.
[40] *ANSYS Electromagnetics Suite—HFSS*, ANSYS, Inc., Canonsburg, PA, USA, 2021.
[41] R. J. Mailloux, *Phased Array Antenna Handbook*, 2nd ed. Norwood, MA, USA: Artech House, 2005.
[42] M. Skolnik and D. King, "Self-phasing array antennas," *IEEE Trans. Antennas Propag.*, vol. AP-12, no. 2, pp. 142–149, Mar. 1964.
[43] C. Pon, "Retrodirective array using the heterodyne technique," *IEEE Trans. Antennas Propag.*, vol. AP-12, no. 2, pp. 176–180, Mar. 1964.
[44] P. Rocca, M. Benedetti, M. Donelli, D. Franceschini, and A. Massa, "Evolutionary optimization as applied to inverse problems," *Inverse Probl.*, vol. 25, Dec. 2009, Art. no. 123003.
[45] G. Oliveri, M. Salucci, and A. Massa, "Features and potentialities of static passive EM skins for NLOS specular wireless links," *IEEE Trans. Antennas Propag.*, vol. 71, no. 10, pp. 8048–8060, Oct. 2023.
[46] S. Hong, Y. Kim, and J. Oh, "Automobile laminated glass window embedded transmitarray and ray tracing validation for enhanced 5G connectivity," *IEEE Trans. Antennas Propag.*, vol. 70, no. 8, pp. 6671–6682, Aug. 2022.
[47] B. Kim and J. Oh, "Single-glass-layer optically transparent transmitarray with high aperture efficiency and low profile at 5G millimeter-wave band," *IEEE Trans. Antennas Propag.*, vol. 71, no. 11, pp. 9036–9041, Nov. 2023.
[48] G. Liu, M. R. D. Kodnoeih, K. T. Pham, E. M. Cruz, D. Gonzalez-Ovejero, and R. Sauleau, "A millimeter-wave multibeam transparent transmitarray antenna at Ka-band," *IEEE Antennas Wireless Propag. Lett.*, vol. 18, pp. 631–635, 2019.
[49] J. Huang and J. A. Encinar, *Reflectarray Antennas*. Hoboken, NJ, USA: Wiley, 2008.

GIACOMO OLIVERI (Fellow, IEEE) received the B.S. and M.S. degrees in telecommunications engineering and the Ph.D. degree in space sciences and engineering from the University of Genoa, Italy, in 2003, 2005, and 2009, respectively. He has been a Visiting Researcher with L2S, in 2012, 2013, and 2015; an Invited Associate Professor with the University of Paris Sud, France, in 2014; and a Visiting Professor with Université Paris-Saclay, in 2016 and 2017. He is currently an Associate Professor with the Department of Civil, Environmental, and Mechanical Engineering, University of Trento, and a Board Member of the ELEDIA Research Center. He is also an Adjunct Professor with CentraleSupélec, Gif-sur-Yvette, France, and a member of the Laboratoire des Signaux et Systemes (L2S), CentraleSupéslec. He is the author/coauthor of over 400 peer-reviewed papers in international journals and conferences. His research work is mainly focused on electromagnetic direct and inverse problems, metamaterials analysis and design, and antenna array synthesis. He has been serving as a member for the IEEE AP-S Field Award Subcommittee and the IEEE AP-S Membership and Benefits Committee. He is the Chair of the IEEE AP/ED/MTT North Italy Chapter. He has been serving as the Chair for the AP-S IEEE Press Liaison Committee. He served as an Associate Editor for IEEE Antennas and Wireless Propagation Letters, from 2016 to 2022, and IEEE Journal on Multiscale and Multiphysics Computational Techniques, from 2017 to 2023. He is an Associate Editor of *EPJ Applied Metamaterials*, *International Journal of Antennas and Propagation*, *International Journal of Distributed Sensor Networks*, *Microwave Processing*, and *Sensors*.

FRANCESCO ZARDI received the B.Sc. degree in telecommunications and electronic engineering and the M.Sc. degree in information and communications engineering from the University of Trento, Italy, in 2017 and 2019, respectively. He attended the International Doctoral School in Information and Communication Technology of Trento. He is currently a Senior Researcher with the ELEDIA Research Center. His research interests include electromagnetic diagnostic techniques, smart electromagnetic environments, and advanced radar architectures.

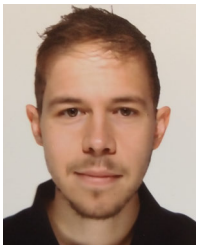

GIORGIO GOTTARDI received the B.S. degree in electronics and telecommunication engineering and the M.S. degree in telecommunication engineering from the University of Trento, Italy, in 2012 and 2015, respectively, and the Ph.D. degree from the International Doctoral School in Information and Communication Technology of Trento, in 2019. He is currently a Postdoctoral Researcher with the Department of Civil, Environmental and Mechanical Engineering (DICAM), University of Trento, and a Research Fellow with the ELEDIA Research Center. His research interest includes synthesis methods for unconventional antenna array architectures for next-generation communications.

ANDREA MASSA (Fellow, IEEE) received the Laurea (M.S.) degree in electronic engineering and the Ph.D. degree in EECS from the University of Genoa, Genoa, Italy, in 1992 and 1996, respectively. He is currently a Full Professor of electromagnetic fields with the University of Trento, where he also teaches electromagnetic fields, inverse scattering techniques, antennas and wireless communications, wireless services and devices, and optimization techniques. He is also the Director of the network of federated laboratories "ELEDIA Research Center" (www.eledia.org), such as ELEDIA@UTB, Bandar Seri Begawan, Brunei; ELEDIA@TSINGHUA, Beijing, China; ELEDIA@UniCAS, Cassino, Italy; ELEDIA@UESTC, Chengdu, China; ElEDIA@UiC, Chicago, USA; ELEDIA@USIL, Lima, Peru; ELEDIA@UniNAGA, Nagasaki, Japan; ELEDIA@L2S, Paris, France; ELEDIA@CTU, Prague, CzechRepublic; ELEDIA@AUTH, Thessaloniki, Greece; ELEDIA@UniTN, Trento, Italy; ELEDIA@Innov'COM, Tunis, Tunisia; and ELEDIA@XIDIAN, Xi'an, China. He is the holder of the Chang-Jiang Chair Professorship with UESTC, Chengdu, China; a Visiting Research Professor with the University of Illinois at Chicago, Chicago; a Visiting Professor with Tsinghua University, Beijing; a Visiting Professor with Tel Aviv University, Tel Aviv, Israel; and a Professor with CentraleSupélec, Paris. He has been the holder of a Senior DIGITEO Chair with L2S-CentraleSupelec and CEA LIST, Saclay, France; the UC3M-Santander Chair of Excellence with the Universidad Carlos III de Madrid, Spain; an Adjunct Professor with Penn State University, USA; a Guest Professor with UESTC; and a Visiting Professor with Missouri University of Science and Technology, USA; Nagasaki University, Japan; the University of Paris Sud, France; Kumamoto University, Japan; and the National University of Singapore, Singapore. He has organized more than 100 scientific sessions at international conferences and has participated in several technological projects in the national and international framework with both national agencies and companies (18 international prj, >5 MEu; eight national prj, >5 MEu; ten local prj, >2 MEu; 63 industrial prj, >10 MEu; six university prj, >300 KEu). He published more than 900 scientific publications among which more than 350 on international journals (>14.700 citations, H-index = 63 [Scopus]; >12.000 citations, H-index = 58 [ISI-WoS]; >23.900 citations, H-index = 88 [Google Scholar]) and more than 570 in international conferences where he presented more than 210 invited contributions (>50 invited keynote speaker) (www.eledia.org/publictos). His research interests include inverse problems, analysis/synthesis of antenna systems and large arrays, radar systems synthesis and signal processing, cross-layer optimization and planning of wireless/RF systems, semantic wireless technologies, system-by-design and material-by-design (metamaterials and reconfigurable-materials), and theory/applications of optimization techniques to engineering problems (telecommunications, medicine, and biology). He is a fellow of IET and Electromagnetic Academy. He is a member of the Editorial Board of the *Journal of Electromagnetic Waves and Applications*, a Permanent Member of the PIERS Technical Committee and the EuMW Technical Committee, and an ESoA Member. He has been appointed to the Scientific Board of the "Società Italiana di Elettromagnetismo (SIEm)" and elected to the Scientific Board of the Interuniversity National Center for Telecommunications (CNIT). In 2011, he was appointed by the National Agency for the Evaluation of the University System and National Research (ANVUR) as a member of the Recognized Expert Evaluation Group (Area 09, Industrial and Information Engineering) for the evaluation of the research at the Italian University and Research Center for the period 2004–2010. Furthermore, he has been elected as the Italian Member of the Management Committee of the COST Action TU1208-Civil Engineering Applications of Ground Penetrating Radar. From 2011 to 2014, he served as an Associate Editor for IEEE TRANSACTIONS ON ANTENNAS AND PROPAGATION. He serves as an Associate Editor for *International Journal of Microwave and Wireless Technologies*. He has been appointed as the IEEE AP-S Distinguished Lecturer, from 2016 to 2018.

Open Access funding provided by 'Università degli Studi di Trento' within the CRUI CARE Agreement